

Suppression of electroosmotic flow by polyampholyte brush

Yuxin Zuo · Guoqiang Wang · Ying Yu ·
Chuncheng Zuo · Zhichao Liu · Dongmei Hu ·
Yirui Wang

Received: 18 November 2013 / Accepted: 2 March 2014 / Published online: 11 March 2014
© Springer-Verlag Berlin Heidelberg 2014

Abstract Molecular dynamics simulations are conducted to investigate the suppression of electroosmotic flow by grafting polyampholyte brushes onto two parallel channel walls. The effects of grafting density and charge distribution of polyampholyte brushes on the electroosmotic flow velocity, salt ion distribution, and conformational characteristics of grafted brushes are studied in detail. Simulation results indicate that increasing the grafting density induces a stronger suppression of electroosmotic flow. The flow velocity is significantly influenced by the different charge distributions of polyampholyte brushes. In addition, an important flow phenomenon we have found is that the flow velocity profile shows a valley at the center of the channel. These results reveal that the flow velocity is dependent not only on the conformation of the polyampholyte brushes but also on the anion and cation distributions. The hierarchical distribution of salt ions is caused by the special properties of polyampholyte brushes.

Keywords Electroosmotic flow · Suppression · Polyampholyte brush · Molecular dynamics

1 Introduction

Fluids in nanochannels can be driven by the external electric field to form electroosmotic flow (EOF). The inner wall of nanochannels becomes negatively charged when in contact with an electrolyte solution. Ionization occurs next

to the surface, which leads to the formation of a charged layer of fluid (Debye layer). The thickness of the Debye layer is affected by the bulk ionic concentration and is considerably less than the channel dimension. The liquid can be dragged by the mobile ions in the diffuse layer because of the potential gradient along the nanochannels (Slater et al. 2010; Subramaniam and Chakraborty 2011). EOF has attracted considerable attention from research institutions because of its numerous applications in the fields of biological analysis and chemical process. For example, EOF has been applied in microfluidic and nanofluidic devices as a pumping method with the fast development of the lab-on-a-chip technology (Stone et al. 2004; Wang et al. 2009). Formation mechanism and control of EOF have attractive interest both in engineering applications and fundamental research (Squires and Quake 2005). Extensive efforts have been exerted to modulate EOF, which is significant for biomolecular separation by electrophoresis. The size of recent fluidic devices for protein or DNA electrophoresis is mostly in nanoscale. EOF drags the fluid at a certain speed along the nanochannels, which is unfavorable to fluid separation. Effective suppression of the EOF velocity can significantly improve the resolution, reproducibility, and efficiency of separation.

Among the numerous methods of modulating electroosmosis, surface modification is crucial in controlling EOF. Messenger and Squires (2010) showed that nanoscale surface roughness can significantly suppress EOF under sufficient excess surface conductivity. Recent research has indicated that polymer brushes can modulate or even eliminate EOF (Chiari et al. 2000; Harden et al. 2001; Horvath and Dolnik 2001; Tessier and Slater 2005; Paumier et al. 2008; Ma et al. 2009; Shendruk et al. 2012; Nii et al. 2013). The effects of polymer brushes on the velocity and direction of EOF have been studied by Boonsong et al.

Y. Zuo · G. Wang · Y. Yu (✉) · C. Zuo · Z. Liu · D. Hu ·
Y. Wang
College of Mechanical Science and Engineering,
Jilin University, Changchun 130022, China
e-mail: yingyu.jlu@gmail.com

(2008). Yasui et al. (2011) found that nanopillar array structures have an intrinsic ability to suppress EOF. Tessier and Slater (2006) and Hickey et al. (2009) investigated the mechanisms by which EOF is modulated by neutral polymer brushes using coarse-grained molecular dynamics (MD) simulations. Their results agree well with experimental observations (Doherty et al. 2002) and confirm the scaling predictions by Harden et al. (2001). The time evolution of the effect of adsorbed polymer coatings on the suppression of EOF was investigated by Hickey et al. (2012) through MD simulations. Compared with neutral polymer brushes, polyelectrolyte brushes have received less attention (Hickey et al. 2011). Polyelectrolyte brushes have various conformations, which can be ascribed to the long-range electrostatic interaction between charged monomers. Our research group previously attempted to modulate EOF by grafting polyelectrolyte brushes onto the inner wall of nanochannels using MD simulations (Cao et al. 2012a, b; Zhang et al. 2012). These simulations showed that the conformation of polyelectrolyte brushes, EOF velocity, and counterion distribution could be significantly affected by different factors, including the solvent quality, normal electric field, charge distribution, and the grafting density of polyelectrolyte brushes.

Previous studies provided insights into the function of neutral polymer or polyelectrolyte brushes with monomers that have the same charge in controlling EOF. Polyampholyte (PA) is a special type of polymer that contains both positive and negative charges. The existence of opposite charges in one chain produces different interesting properties compared with polymer or polyelectrolytes layers. The properties of the PA chain in solutions principally depend on the composition (including positive, negative, and neutral monomer), charge density, and distribution of charged monomers along the polymer backbone. Experiments have shown that PA chains can be used to form polymer brushes (Osborne et al. 2002; Yu et al. 2007; Kitano et al. 2011). Baratlo and Fazli (2009) used MD simulations to study neutral PA brushes with different sequences of charged monomers at various grafting densities. PA brushes can respond to numerous internal and external stimuli (Qu et al. 2011), such as electric field, temperature, salt concentration, pH, and PA grafting density. Varying these stimuli can produce PA brushes with different conformations and, consequently, different surface properties. However, to the best of our knowledge, few studies have focused on suppressing EOF using neutral PA brushes. We have investigated the suppression of EOF in a nanochannel grafted with polyelectrolyte brushes under the control of a normal electric field to channel wall (Cao et al. 2012a, b). Accordingly, we have performed MD simulations for EOF suppression in a PA-grafted channel using PA chains with different grafting densities and charge distributions. Results of the current

study reveal that the flow velocity profile shows a valley at the center of the channel. A similar flow feature was observed in previous studies. Tang and colleagues reported the results of EOF in a nanopore using density functional theory combined with continuum Navier–Stokes equations. Their study shows that charge inversion reduces EOF velocity and even leads to flow reversal in high salt concentration (Tang and Hu 2013). Hickey et al. (2009) studied the suppression of EOF using a dynamically adsorbed polymer coating. Their investigation shows that the optimal adsorption strength to suppress EOF is similar to the transition of polymer adsorption.

The rest of this paper is organized as follows. Details of the model system and MD method are described in Sect. 2. The results are discussed and presented in Sect. 3. Finally, conclusions are provided in Sect. 4.

2 Model and simulation method

2.1 Modeling

We conducted MD simulations of a coarse-grained model, which is well established for the investigation of EOF suppression using PA brushes. The confining walls are represented by rigid, face-centered cubic crystalline surfaces. The wall atoms remain at fixed relative positions and do not interact with other particles. The charged particles are chosen from the wall atoms in the first layer. One end of the PA brushes with N monomers is grafted onto a surface and arranged in a square lattice with the spacing $d = \rho_g^{-1/2}$, where ρ_g is the number of grafted brushes per unit area. The number of monomer beads on each PA chain is $N = 9$. Charged monomers of the opposite sign with equal numbers are arranged along the PA chain, whereas the others are neutral. Different distributions and quantities of charged monomers (Fig. 1) in PA brushes are discussed in this paper. Counterions are added into the nanochannel to neutralize the system in accordance with the method proposed by Cao et al. (2009) and Hehmeyer and Stevens (2005). In addition, solvent particles including salt ions and water are added randomly in the nanochannel. A nanofluidic channel coated with PA brushes is schematically shown in Fig. 2.

All particles in the system interact via the truncated-shifted Lennard–Jones (LJ) potential,

$$U_{\text{LJ}}(r) = 4\varepsilon_{\text{LJ}}[(\sigma/r)^{12} - (\sigma/r)^6 - (\sigma/r_c)^{12} + (\sigma/r_c)^6], \quad r < r_c \quad (1)$$

where r is the distance between two particles; ε_{LJ} and σ are LJ parameters; r_c denotes the cut-off radius; and m , ε_{LJ} , and σ are the units of mass, energy, and length, respectively. All other units are obtained from the basic units, such as the velocity unit $u^* = (\varepsilon_{\text{LJ}}/m)^{1/2}$, electric field unit

Fig. 1 Polyampholyte brushes with different charge distributions

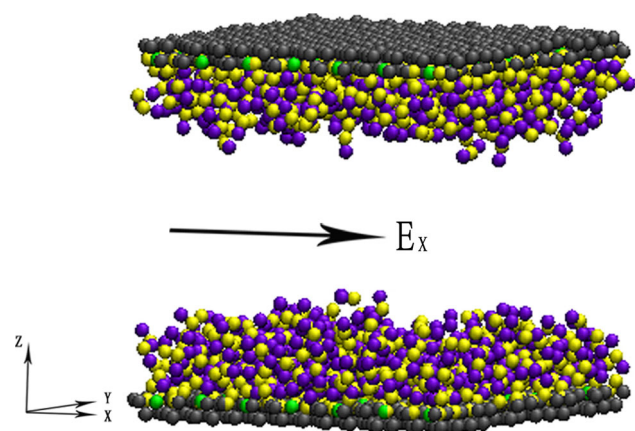
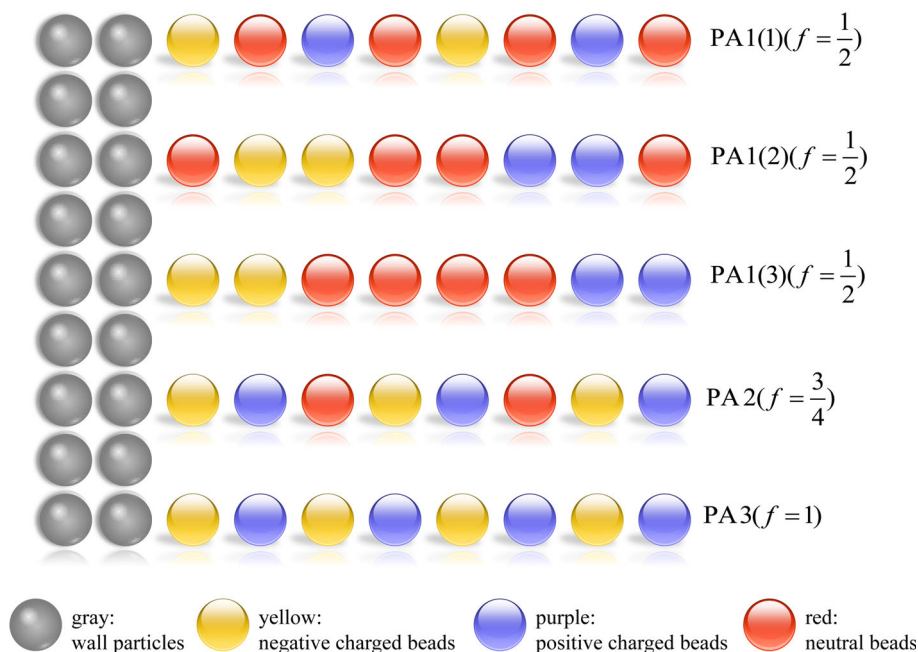


Fig. 2 Visual snapshots from MD simulations of EOF confined between two parallel planar surfaces at $E/E^* = 1.0$ and $\rho_g \sigma^2 = 0.29$. For simplicity, all of the mobile particles, including solvent particles, added salt ions, and counterions, are not shown. The PA brushes shown in this figure are represented by PA1, and the purple and yellow beads represent positively and negatively charged monomers, respectively. The wall beads consist of gray neutral and green charged ones (color figure online)

$E^* = \epsilon_{LJ} \sigma^{-1} / (4\pi \epsilon_0 \sigma \epsilon_{LJ})^{1/2}$ (ϵ_0 is the vacuum permittivity), time unit $\tau = (m \sigma^2 / \epsilon_{LJ})^{1/2}$, and temperature unit $T^* = \epsilon_{LJ} / k_B$ (k_B is the Boltzmann constant).

The bonds of PA chains are modeled using a finitely extensive nonlinear elastic potential (FENE) (Kremer and Grest 1990).

$$U_{\text{bond}}(r) = -(kR_0^2/2) \ln(1 - r^2/R_0^2) \tag{2}$$

with the maximum bond length $R_0 = 1.5\sigma$ and the spring constant $k = 30\epsilon_{LJ}/\sigma^2$. The equilibrium bond length $a = 0.98\sigma$ is obtained by minimizing $U_{LJ}(r) + U_{\text{bond}}(r)$.

The Coulomb interaction between any two charged particles (charged monomers, counterions, salt ions, and part of wall particles) is included as

$$U_{\text{Coul}}(r_{ij}) = k_B T Z_i Z_j \frac{\lambda_B}{r_{ij}} \tag{3}$$

where r_{ij} is the distance between charged particles i and j , and Z_i and Z_j are charges on two particles in units of an electron charge. $\lambda_B = e^2 / (4\pi \epsilon_0 \epsilon_r k_B T)$ is the Bjerrum length, defined as the length scale at which the electrostatic energy between two elementary charges e in a dielectric medium with the dielectric constant ϵ_r is comparable in magnitude with the thermal energy $k_B T$. In our simulations, the particle–particle particle–mesh (PPPM) algorithm, which maps the charge of 3D mesh, is used to calculate the sum of all long-range Coulomb interactions. We adopted the PPPM algorithm proposed by Beckers et al. (1998). The same algorithm was used by Liu et al. (2010) to simulate the electroosmotic flows in rough nanochannels. The basic idea of the PPPM algorithm is to split the Coulomb potential into a short range direct interaction part (PP) and a contribution from the mesh (PM).

$$U_i = \sum_{j < i} U_{ij}^{\text{direct}} + U_i^{\text{mesh}} \tag{4}$$

The direct part of the Coulomb potential is given by

$$U_{ij}^{\text{direct}}(r_{ij}) = \begin{cases} e_i e_j \left(\frac{1 - U^c(r_{ij})}{4\pi \epsilon |r_{ij}|} \right) & r_{ij} \leq r_c \\ 0 & r_{ij} \geq r_c, \end{cases} \tag{5}$$

where r_c is the direct interaction cut-off radius, and $U^c(r_{ij})$ is the correction term used to compensate for the portion of

interaction already covered by the mesh potential. The mesh potential can be written as

$$U_i^{\text{mesh}} = e_i \sum_k H(R_i - R_k) \phi(R_k) - U^{\text{self}}, \quad (6)$$

where H is the weight of a charge particle located at R . $\phi(R)$ is the electrostatic potential at grid point R , and U^{self} is a correction term for the mesh potential which a particle experiences from its own charge distribution. The PPPM algorithm uses fast Fourier transforms (FFTs) to solve Poisson's equation on the mesh (Hockney and Eastwood 1988). The original PPPM algorithm is used in periodic systems. Calculating the Coulomb interactions in systems with slab geometry, which are periodic in x and y directions and have a finite length in the z direction, requires removal of artificial periodicity along the z direction by extending the PPPM mesh with empty volume in the z direction with the height of $3L_z$. A correction term is also added to the modified PPPM algorithm (Yeh and Berkowitz 1999).

2.2 Simulation details

The simulation box has volume $L_x \times L_y \times L_z$, where $L_x = L_y = 22.2\sigma$ and $L_z = 24.3\sigma$. Periodic boundary conditions are applied along the x and y directions, whereas the z direction has a fixed boundary. In all simulations, the density of the mean fluid particles filling the space between the substrates is $\rho_f = 0.81\sigma^{-3}$, the salt concentration is $\rho_s = 0.02\sigma^{-3}$, the wall density is $\rho_w = 1.0\sigma^{-3}$, and the surface charge density is $\rho_c = -0.1\sigma^{-3}$ (charges on both surfaces are negative). The PA chains are grafted on each substrate. An electric field E is applied parallel to the channel walls to induce the translational motion of charged beads. The dimensionless electric field E/E^* is fixed at 1.0. An athermal system is used in this study to make all pair interactions purely repulsive. The cut-off radius and length unit are assigned as $r_c = 2^{1/6}\sigma$ and $\sigma = 0.3$ nm, respectively.

The system temperature is maintained at $T = 1.2T^*$ using a dissipative particle dynamics (DPD) thermostat (Hoogerbrugge and Koelman 1992; Español and Warren 1995) with a friction coefficient $\gamma = 1.5\tau^{-1}$. The Bjerrum length is fixed at $\lambda_B = 2\sigma$, and the desired temperature is $T = 300$ K. The velocity Verlet algorithm with a time step $\Delta t = 0.005\tau$ is used to calculate the positions and velocities of the particles. For each simulation, 5×10^5 time steps are first performed to reach equilibrium state. Another 5×10^5 time step runs are necessary to sample the simulation data.

3 Results and discussion

This section enumerates the effects of the grafting density and charge distribution of the PA chains on flow

characteristics. First, we investigated the different charge distribution of the PA chain with fixed charge fraction $f = \frac{1}{2}$ at $\rho_g\sigma^2 = 0.29$. The EOF velocity profiles are shown in Fig. 3. For simplicity, only half of the channel is shown because the system is symmetrical. In this figure, EOF is suppressed more apparently in the case of PA1 (1) compared with PA1 (2) and PA1 (3). The density profiles of monomer beads are presented in Fig. 4 (the arrows denote the average thickness of PA brushes). The PA brushes with blocks of similarly charged monomers, PA1 (2) and PA1 (3), have buckled conformations and are pressed against the grafting surface because of the strong electrostatic attractions. For the PA1 (1) brushes, the charged monomers have uniform distribution along the chains. The electrostatic neutrality is satisfied in smaller length scales, and the electrostatic correlations between the chains are weaker than in PA1 (2) and

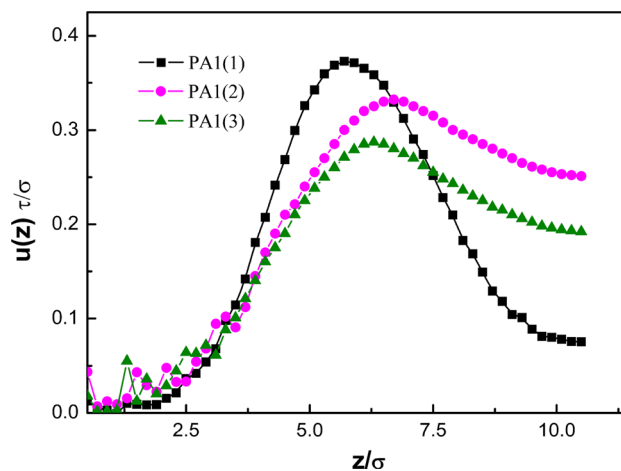


Fig. 3 Velocity profiles in channel at $\rho_g\sigma^2 = 0.29$ for different charge distributions of PA1 chains at fixed charge fraction $f = \frac{1}{2}$

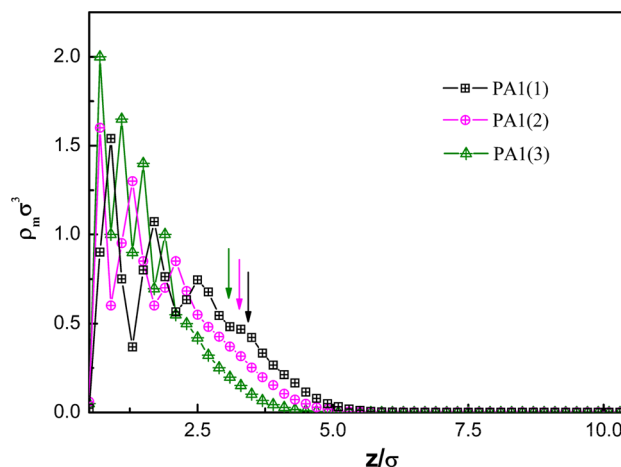


Fig. 4 Monomer density profiles at $\rho_g\sigma^2 = 0.29$ for different charge distributions of PA1 chains at fixed charge fraction $f = \frac{1}{2}$. Arrows denote the average thickness of PA brushes

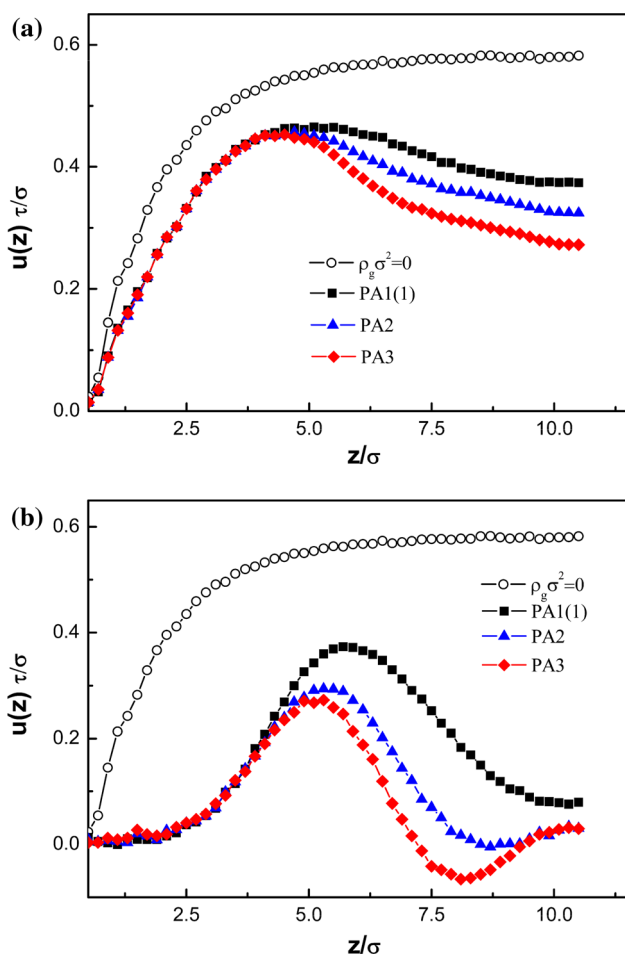


Fig. 5 Velocity profiles at different grafting densities: **a** $\rho_g\sigma^2 = 0.05$ and **b** $\rho_g\sigma^2 = 0.29$ for different charge distributions of PA chains. The circles represent the case without polymer coating

PA1 (3). Comparing the thickness of these three kinds of PA brushes, we found that PA1 (1) is thicker than the two other brushes. Meanwhile, the amount of solvent particles within the brush layer is higher than that in the two other cases, which causes more solvent particles to move toward the electrical double layer close to the wall. The thicker PA layer also leads to long-range decay of the EOF velocity. In this study, we focus mainly on the PA brushes with charged monomers that are distributed uniformly.

Figure 5 presents the velocity profiles for different charge distributions of PA brushes at $\rho_g\sigma^2 = 0.05$ and 0.29 . The circled line represents the case without PA brushes. A plug-like velocity profile of EOF can be observed in the bare nanochannel (i.e., the channel without grafted polymer brushes). A similar phenomenon is also observed in the literatures (Cao et al. 2010a, b; Tessier and Slater 2006). The shape of the velocity profiles of the channel surface grafted with PA brushes is obviously different from that of the bare channel (Fig. 5). The EOF is also suppressed visibly in the former.

At a low grafting density of $\rho_g\sigma^2 = 0.05$, the flow velocity is almost the same in the region of $z < 4.5\sigma$ with different charge distributions of PA brushes grafted on the nanochannel, whereas the velocity in the other region is significantly reduced. In our simulation, different charge distributions of PA chains have different charge fractions f . The flow velocity at the center of the channel is decreased as the charge fraction of the PA brushes is increased. At the highest grafting density of $\rho_g\sigma^2 = 0.29$, the shape of the velocity profile is markedly changed. The flow velocity profile in the region of $5\sigma < z < 10\sigma$ shows a sharp peak; a low valley is also observed at the center of the channel. As shown in Fig. 5, the increase in the charge fraction of PA brush leads to a stronger suppression of EOF. For PA3, the flow velocity shows significantly negative values in the region of $7\sigma < z < 9\sigma$ where EOF is almost completely suppressed, and the velocity rises slightly at the center of the channel. Snapshots show that the anchored PA brushes adopt a collapsed conformation. The strong electrostatic interactions between charged monomers link the brushes to each other. This finding reveals that the collapse of PA brushes induces normal stress toward the wall and surface friction between ions and walls, which further suppresses the movement of ions or the EOF transport. Under certain conditions (when the channel is coated with polyelectrolytes or neutral polymer brushes), the EOF velocity is relatively high at the center region of a channel along the z direction (Cao et al. 2010; Zhang et al. 2012). This result can be attributed to the lack of hindrance in polymer brushes. In this study, the velocity profile showed a low valley at the center region of a channel, regardless of whether the grafting density was low or high. A similar flow feature was observed in previous research (Hickey et al. 2009; Tang and Hu 2013). This phenomenon indicates that the change in EOF velocity depends not only on the conformation of PA brushes but also on the salt ion distribution.

For the PA-grafted wall, the flow near the wall becomes more complex because of the superposition of the boundary Debye layer and the PA ion layer. Figures 6 and 7 show the salt ion density profiles at $\rho_g\sigma^2 = 0.05$ and $\rho_g\sigma^2 = 0.29$ for various charge distributions of PA brushes. The grafting density of PA brushes and the charge distribution significantly affect the ion distribution. At $\rho_g\sigma^2 = 0.05$, cations aggregate out of the brush layer. However, a considerable part of the anions is in the brush layer. As the charge fraction of PA brushes is increased, more cations are distributed in the region of $3\sigma < z < 5\sigma$, whereas more anions gather at the center of the nanochannel. The densities of the anions and cations at a high grafting density of $\rho_g\sigma^2 = 0.29$ show a different distribution compared with those at $\rho_g\sigma^2 = 0.05$. The salt ion density profiles show that cations are distributed less in

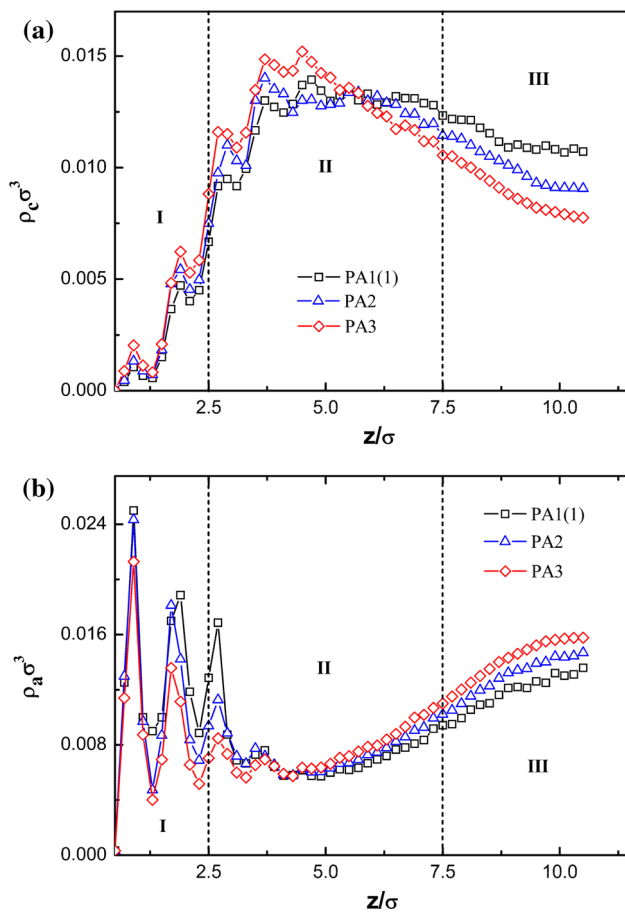


Fig. 6 Density profiles of **a** cations and **b** anions for PA-grafted channels at $\rho_g\sigma^2 = 0.05$ with different charge fractions

region $7\sigma < z < 9\sigma$ for the case of PA3, and the EOF velocity profiles indicate an obvious drop. This condition shows that in the region where numerous cations are distributed, the EOF velocity is relatively larger than that in other regions. We believe that ion distribution should have a considerable effect on the EOF. This effect can be attributed to the electric field E that drives the migration of ions, which induces the motion of surrounding fluid particles. One can observe that only a small amount of salt ions is distributed near the wall. That is, most ions are in a wide region away from the wall. Two effects contribute to this behavior. First, with increasing grafting density, a growing number of charged monomers form a compact PA layer near the wall because of the electrostatic interactions. Second, excluded volume effects cause difficulty for most salt ions to penetrate the brush layer and approach the wall. The salt ion density profiles show that the salt ions have a hierarchical distribution in the z direction. In the region where a large quantity of anions is distributed, a relatively small number of cations is distributed. Basing on the uneven distribution of salt ions, we partition the channel into I, II, and III along the channel width direction (Fig. 6).

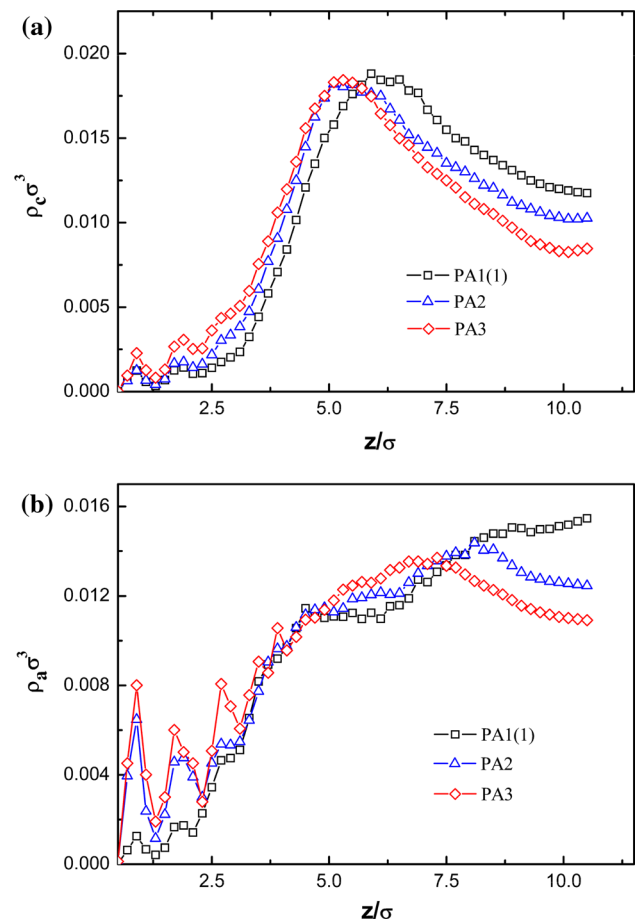


Fig. 7 Density profiles of **a** cations and **b** anions for PA-grafted channels at $\rho_g\sigma^2 = 0.29$ with different charge fractions

We also calculate the aggregate amount of salt ions $M\sigma^2$ in each region in Fig. 8 (for example, $\rho_g\sigma^2 = 0.05$). As the charge fraction of PA chains is increased, the hierarchical phenomenon of salt ions becomes more obvious.

These data suggest that increasing the grafting density and charge fraction of PA brushes can affect the distribution of salt ions along the direction normal to the channel wall and may decrease electroosmotic velocity. Thus, EOF can be controlled by different mechanisms in nanochannels coated with PA chains, which causes the fluid to exhibit more complex flow characteristics. In contrast to traditional EOF, obtaining fundamental laws governing EOF with PA brushes and expression of salt ion distribution is difficult.

Figure 9 presents the density profiles of a monomer at high grafting density $\rho_g\sigma^2 = 0.29$. Apart from the salt ion distribution, the polymer coverage also has a significant function in controlling the EOF, particularly at high grafting density. The neutrally, positively, and negatively charged monomers are analyzed statistically. High monomer density occurs near the wall. The significant oscillation shown in the density profile is mainly induced by the ordering layer structure of wall particles. In this figure, the

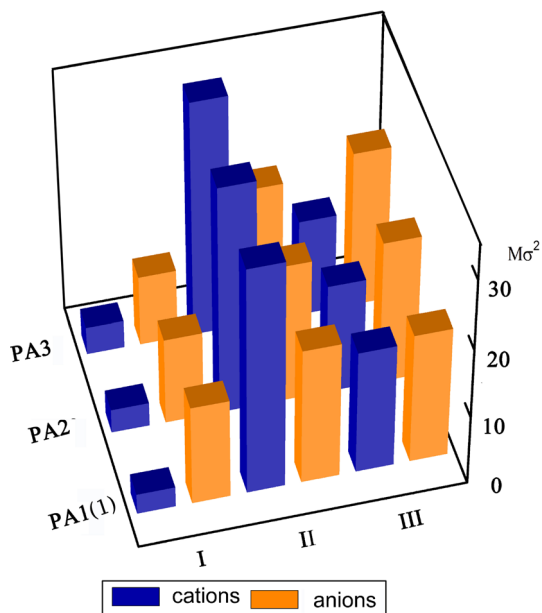


Fig. 8 Aggregate amount of cations and anions in regions I, II, and III at $\rho_g \sigma^2 = 0.05$

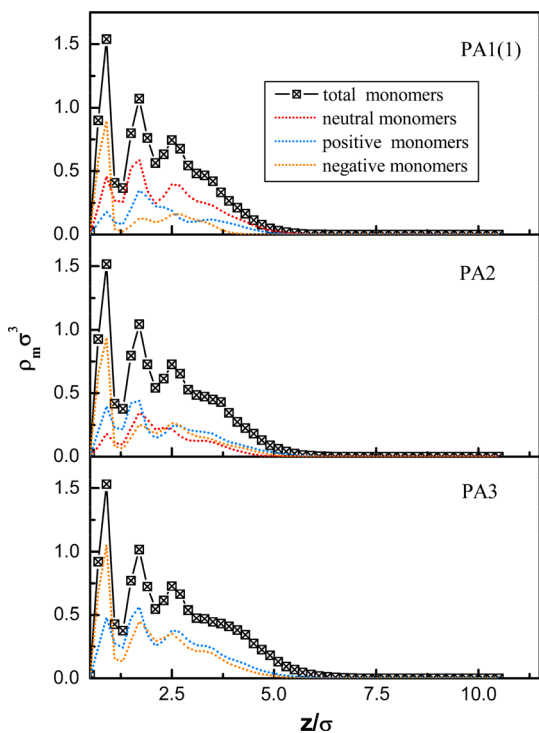


Fig. 9 Monomer density at $\rho_g \sigma^2 = 0.29$ for different charge distributions; the neutrally, positively, and negatively charged monomers are analyzed statistically

staggered distribution of positively and negatively charged monomers near the channel surface is shown. This condition is one of the main reasons why a hierarchical distribution of salt ions is necessary.

To study the effective width of the channel quantitatively, we calculate the average thickness of the grafted layer using the following formula:

$$h = \frac{\int_0^{L_z} z \rho_{m1}(z) dz}{\int_0^{L_z} \rho_{m1}(z) dz} \tag{7}$$

where ρ_{m1} is the monomer density of the bottom PA brushes. Figure 10 shows the brush thickness h as a function of the grafting density with different charge distributions of PA chains. Increasing the grafting density or charge fraction of the PA chains evidently induces an increase in h . A similar behavior has been observed for neutral polymer brushes. The increase in the brush layer thickness can diminish the size of the channels and limit the volume flux. With increasing grafting density, the amount of fluid particles excluded from the PA layer increases because of the interchain attraction. Most counterions are outside the brush because the net charge of the PA chain is zero. The average thickness of the PA brushes is mainly determined by the excluded volume effects. In polymer brushes, increased thickness with increasing grafting density is typical behavior (Cao et al. 2010a, b). For polyelectrolyte brushes, the conformation is determined by the competition between electrostatic repulsion among the chains and moderation of this effect by counterions that screen the interactions among electrolyte monomers. The horizontal electric field is also crucial in controlling the thickness of PA brushes because of the shear force induced by the particle motion driven by the horizontal electric field, as in the case of EOF modulated by polymer brushes (Binder 2002; Cao et al. 2010). We fixed the horizontal electric field in this study; that is, the effect of the horizontal electric field is not discussed.

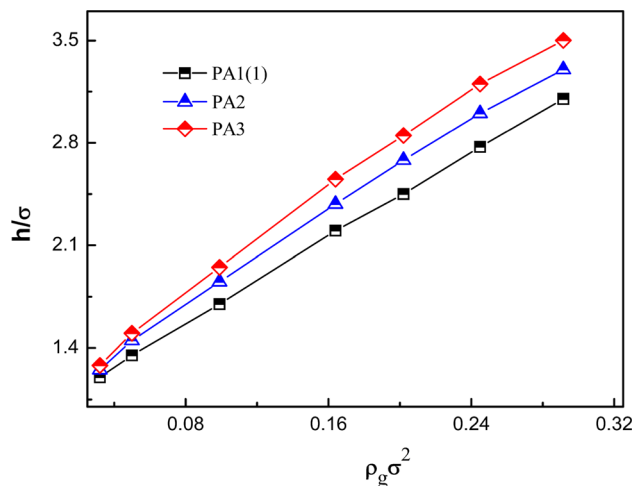


Fig. 10 Average thickness h of PA brushes as a function of grating density with different charge distributions

4 Conclusion

The suppression of EOF in a nanofluidic channel grafted with PA brushes is studied using MD simulation. The combination effects of the grafting density $\rho_g \sigma^2$ and charge distribution on flow characteristics are addressed. The hierarchical distribution of salt ions along the channel width induced by the special properties of PA brushes has a significant effect on the shape of velocity profiles. EOF is significantly suppressed under high grafting density. Certain results obtained in this study agree with previous simulation results. The flow velocity profile shows a valley at the center of the channel. This novel result is crucial to studies focusing on biomolecular separation, reproducibility improvement, and so on. In our study, parameters such as salt concentration, solvent quality, and electric field strength are fixed. However, the effects of these parameters on EOF are not determined in this study. In the future, we will perform further simulations and experiments to present a detailed report.

Acknowledgments This work was supported by the National Natural Science Foundation of China (No. 51175223) and the Science and Technology Planning Project of Jilin Province (No. 20100564).

References

- Baratlo M, Fazli H (2009) Molecular dynamics simulation of semiflexible polyampholyte brushes—the effect of charged monomers sequence. *Eur Phys J E* 29:131–138. doi:10.1140/epje/i2009-10458-x
- Beckers JVL, Lowe CP, De Leeuw SW (1998) An iterative PPPM method for simulating coulombic systems on distributed memory parallel computers. *Mol Simul* 20:369–383. doi:10.1080/08927029808022044
- Binder K (2002) Scaling concepts for polymer brushes and their test with computer simulation. *Eur Phys J E* 9:293–298. doi:10.1140/epje/i2002-10076-2
- Boonsong K, Caulum MM, Dressen BM, Chailapakul O, Croke DM, Henry CS (2008) Influence of polymer structure on electroosmotic flow and separation efficiency in successive multiple ionic layer coatings for microchip electrophoresis. *Electrophoresis* 29:3128–3134. doi:10.1002/elps.200800186
- Cao QQ, Zuo CC, He HW, Li LJ (2009) A molecular dynamics study of two apposing polyelectrolyte brushes with mono- and multivalent counterions. *Macromol Theory Simul* 18:441–452. doi:10.1002/mats.200900037
- Cao QQ, Zuo CC, Li LJ (2010) Electroosmotic flow in a nanofluidic channel coated with neutral polymers. *Microfluid Nanofluid* 9:1051–1062. doi:10.1007/s10404-010-0620-5
- Cao QQ, Zuo CC, Li LJ, Zhang YH, Yan G (2012a) Electro-osmotic flow in nanochannels with voltage-controlled polyelectrolyte brushes: dependence on grafting density and normal electric field. *J Polym Sci Pol Phys* 50:805–811. doi:10.1002/polb.23069
- Cao QQ, Zuo CC, Li LJ, Zhang YH (2012b) Modulation of electroosmotic flow by electric field-responsive polyelectrolyte brushes: a molecular dynamics study. *Microfluid Nanofluid* 12:649–655. doi:10.1007/s10404-011-0865-7
- Chiari M, Cretich M, Damin F, Ceriotti L, Consonni R (2000) New adsorbed coatings for capillary electrophoresis. *Electrophoresis* 21:909–916
- Doherty EAS, Berglund KD, Buchholz BA, Kourkine IV, Przybycien TM, Tilton RD, Barron AE (2002) Critical factors for high-performance physically adsorbed (dynamic) polymeric wall coatings for capillary electrophoresis of DNA. *Electrophoresis* 23:2766–2776
- Español P, Warren P (1995) Statistical mechanics of dissipative particle dynamics. *Europhys Lett* 30(4):191–196
- Harden JL, Long D, Ajdari A (2001) Influence of end-grafted polyelectrolytes on electro-osmosis along charged surfaces. *Langmuir* 17:705–715. doi:10.1021/la000594j
- Hehmeyer OJ, Stevens MJ (2005) Molecular dynamics simulations of grafted polyelectrolytes on two apposing walls. *J Chem Phys* 122:134909. doi:10.1063/1.1871937
- Hickey OA, Harden JL, Slater GW (2009) Molecular dynamics simulations of optimal dynamic uncharged polymer coatings for quenching electro-osmotic flow. *Phys Rev Lett* 102:108304. doi:10.1103/PhysRevLett.102.108304
- Hickey OA, Holm C, Harden JL, Slater GW (2011) Influence of charged polymer coatings on electro-osmotic flow: molecular dynamics simulations. *Macromolecules* 44(23):9455–9463. doi:10.1021/ma201995q
- Hickey OA, Harden JL, Slater GW (2012) Computer simulations of time-dependent suppression of EOF by polymer coatings. *Microfluid Nanofluid* 13:91–97. doi:10.1007/s10404-012-0944-4
- Hockney RW, Eastwood JW (1988) Computer simulation using particles. Adam Hilger, Bristol
- Hoogerbrugge PJ, Koelman JMVA (1992) Simulating microscopic hydrodynamic phenomena with dissipative particle dynamics. *Europhys Lett* 19(3):155–160
- Horvath J, Dolnik V (2001) Polymer wall coatings for capillary electrophoresis. *Electrophoresis* 22:644–655
- Kitano H, Kondo T, Kamada T, Iwanaga S, Nakanura M, Ohno K (2011) Anti-biofouling properties of an amphoteric polymer brush constructed on a glass substrate. *Colloid Surf B* 88:455–462. doi:10.1016/j.colsurfb.2011.07.029
- Kremer K, Grest GS (1990) Dynamics of entangled linear polymer melts: a molecular-dynamics simulation. *J. Chem Phys* 92:5057–5086. doi:10.1063/1.458541
- Liu J, Wang M, Chen S, Robbins MO (2010) Molecular simulations of electroosmotic flows in rough nanochannels. *J Comput Phys* 229(20):7834–7847. doi:10.1016/j.jcp.2010.06.042
- Ma D, Chen HW, Shi DY, Li ZM, Wang JF (2009) Preparation and characterization of thermo-responsive PDMS surfaces grafted with poly (N-isopropylacrylamide) by benzophenone-initiated photopolymerization. *J Colloid Interface Sci* 332:85–90. doi:10.1016/j.jcis.2008.12.046
- Messinger RJ, Squires TM (2010) Suppression of electro-osmotic flow by surface roughness. *Phys Rev Lett* 105:144503. doi:10.1103/PhysRevLett.105.144503
- Nii K, Sueyoshi K, Otsuka K, Takai M (2013) Zone electrophoresis of proteins in poly(dimethylsiloxane) (PDMS) microchip coated with physically adsorbed amphiphilic phospholipid polymer. *Microfluid Nanofluid* 14:951–959. doi:10.1007/s10404-012-1102-8
- Osborne VL, Jones DM, Huck WTS (2002) Controlled growth of triblock polyelectrolyte brushes. *Chem Commun* 17:1838–1839. doi:10.1039/B204737C
- Paumier G, Sudor J, Gue AM, Vinet F, Li M, Chabal YJ, Estève A, Djafari-Rouhani M (2008) Nanoscale actuation of electrokinetic flows on thermoreversible surfaces. *Electrophoresis* 29:1245–1252. doi:10.1002/elps.200700396
- Qu LJ, Man XK, Han CC, Qiu D, Yan DD (2011) Responsive behaviors of diblock polyampholyte brushes within self-consistent field theory. *J Phys Chem B* 116:743–750. doi:10.1021/jp210165t

- Shendruk TN, Hickey OA, Slater GW, Harden JL (2012) Electro-phoresis: when hydrodynamics matter. *Curr Opin Colloid Interface Sci* 17:74–82. doi:10.1016/j.cocis.2011.08.002
- Slater GW, Tessier F, Kopecka K (2010) The electroosmotic flow (EOF). *Microeng Biotechnol* 583:121–134. doi:10.1007/978-1-60327-106-6_5
- Squires TM, Quake SR (2005) Microfluidics: fluid physics at the nanoliter scale. *Rev Mod Phys* 77:977–1026
- Stone HA, Stroock AD, Ajdari A (2004) Engineering flows in small devices: microfluidics toward a lab-on-a-chip. *Annu Rev Fluid Mech* 36:381–411. doi:10.1146/annurev.fluid.36.050802.122124
- Subramaniam K, Chakraborty S (2011) A semi-analytical model for species transport in combined electroosmotic and pressure driven microflows with surface adsorption-desorption reactions. *Microfluid Nanofluid* 10:821–829. doi:10.1007/s10404-010-0713-1
- Tang WY, Hu GH (2013) Prediction of the effective force on DNA in a nanopore based on density functional theory. *RSC Adv* 3:19861–19865. doi:10.1039/c3ra43325k
- Tessier F, Slater GW (2005) Control and quenching of electroosmotic flow with end-grafted polymer Chains. *Macromolecules* 38:6752–6754. doi:10.1021/ma0508404
- Tessier F, Slater GW (2006) Modulation of electroosmotic flow strength with end-grafted polymer chains. *Macromolecules* 39:1250–1260. doi:10.1021/ma0522211
- Wang XY, Cheng C, Wang SL, Liu SR (2009) Electroosmotic pumps and their applications in microfluidic systems. *Microfluid Nanofluid* 6:145–162. doi:10.1007/s10404-008-0399-9
- Yasui T, Kaji N, Mohamadi MR, Okamoto Y, Tokeshi M, Horiike Y, Baba Y (2011) Electroosmotic flow in microchannels with nanostructures. *ACS Nano* 5:7775–7780. doi:10.1021/nn2030379
- Yeh IC, Berkowitz ML (1999) Ewald summation for systems with slab geometry. *J Chem Phys* 111:3155–3162. doi:10.1063/1.479595
- Yu K, Wang HF, Xue LJ, Han YC (2007) Stimuli-responsive polyelectrolyte block copolymer brushes synthesized from the Si wafer via atom-transfer radical polymerization. *Langmuir* 23:1443–1452. doi:10.1021/la062159g
- Zhang Z, Zuo CC, Cao QQ, Ma YH, Chen SQ (2012) Modulation of electroosmotic flow using polyelectrolyte brushes: a molecular dynamics study. *Macromol Theory Simul* 21:145–152. doi:10.1002/mats.201100081